PHYSICAL REVIEW B **87**, 184112 (2013)

Pressure impact on the structure, elasticity, and electron density distribution of $CaSi_2O_5$

Yonggang G. Yu,[1,*] Ross J. Angel,[2] Nancy L. Ross,[3] and G. V. Gibbs[3]

[1]*Institute of Geosciences, University of Frankfurt, Altenhöferallee 1, 60438 Frankfurt am Main, Germany*

[2]*Dipartimento di Geoscienze, Università di Padova, Via Gradenigo 6, 35131 Padova, Italy*

[3]*Department of Geosciences, Virginia Polytechnic Institute and State University, Blacksburg, Virginia 24060, USA*

(Received 1 March 2013; published 21 May 2013)

Ab initio molecular dynamics simulations were used to reveal the mechanism of the fivefold to sixfold transition in Si coordination numbers of $CaSi_2O_5$. The longest first-neighbor Si-O distance drops from 2.8 to 1.8 Å upon the triclinic to monoclinic transition. We find significant bulk modulus softening during the structure crossover, which is due to appearance of intermediate Si-O connections in the triclinic phase under slightly nonhydrostatic stress. Nonetheless, no soft phonon modes were found in either structure, indicating that both structures are dynamically stable. Across the transition, c_{33} doubles and c_{35} increases sixfold in magnitude due to the formation of new Si-O bonds. Chemical bonding analysis reveals distinctions in the electron localization function and bond ellipticity between the regular (1.8 Å) and the dangling Si-O bonds (2.8 Å), both of which suggest an impending disassociation of the dangling Si-O bond.

DOI: 10.1103/PhysRevB.87.184112 PACS number(s): 64.70.kp, 61.66.Fn, 62.50.−p

I. INTRODUCTION

The discovery of coexisting fivefold and sixfold coordinated silicon atoms in the triclinic polymorph of $CaSi_2O_5$ (Ref. 1) opened the opportunity to explore in a crystalline material one of the critical steps in the process of pressure-induced amorphization, a phenomenon of wide interest found in materials including ice, silica (SiO_2),[2,3] $AlPO_4$,[4] and zeolites. An amorphous phase, which lacks long-range atomic order (LRO), is thought to be metastable and nonergodic because its energy landscape exhibits multiple local minima.[5] One viable path for amorphization is elastic and/or vibrational instabilities that destabilize crystal structures; for example, close to amorphization, LRO sharply reduces to zero and a wide range of low-frequency vibrational modes arise in phonon spectra. As a result, sharp contrasts may occur in amorphous solids including changes in volume, density, mechanical properties (elasticity), electrical (resistivity) and optical properties. Amorphous materials, such as $AlPO_4$, have been shown to possess a "memory" that preserves its crystalline structure and lattice orientation when decompressed from its high-pressure amorphous state.[4] More recently phase change materials (PCMs) such as $Ge_2Sb_2Te_5$ (GST) have found interesting applications as programmable memory bits, capable of reversibly switching between amorphous and crystalline structures at a remarkably low electric power consumption.[6] In structural biology, organisms can utilize biogenic amorphous calcium carbonate (ACC) as a transient precursor phase to build crystals of desired shapes and polymorphs (calcite and aragonite), such as for mollusk shells.[7] Amorphous materials are ubiquitous in meteorites in which they are formed by shock-induced amorphization, and can be produced in laboratory controlled high-pressure devices such as diamond-anvil cells. There were once speculations associating the amorphization of serpentine, a hydrous mineral in subducting lithosphere, with deep-focus earthquakes (100 to 660 km depth) in the mantle.[8]

The fascinating phenomena arising from amorphization transformations have stimulated intensive studies in the field, including structural characterizations using x-ray and neutron diffraction, Raman and infrared spectroscopy, and large scale molecular dynamics simulations. Although previous studies on ZrW_2O_8,[9] a well known flexible framework structure that contracts when heated, have shed light on the problem by suggesting the connection between amorphization and negative thermal expansion, the detailed mechanism of amorphization is in general still not well understood. In particular, while it is clear that the incipient step of the amorphization in which LRO breaks must involve the breakdown and reformation of chemical bonds, we do not know how this happens. How this incipient process proceeds is also critical for understanding the precursor steps for melting, crystallization, and vitrification as well as atom diffusion in melts.

In this study we approach this problem from a different angle. There exists in nature a crystalline material $CaSi_2O_5$ which is a unique system for studying the incipience of amorphization, because the two polymorphs of $CaSi_2O_5$ convert into each other reversibly at moderate pressure (0.2 GPa) and stress conditions and, in conjunction, a silicon-oxygen (Si-O) bond switches on (∼1.8 Å) and off (∼2.8 Å) when conversions occur. This remarkable material permits a comprehensive theoretical investigation on the Si-O bond formation and rupture in crystalline phases, their influence on elasticity and structural stability, the quantum mechanical nature of the regular and elongated Si-O bonds, and the implications for amorphization. It also allows us to explore whether the assumption of conventional crystal chemistry that such a long Si-O distance is completely nonbonded is valid. However, since their first unambiguous characterization through single-crystal x-ray diffraction experiments,[1] only limited efforts have been devoted to understanding this system. For example, Warren *et al.*[10] have analyzed covalent bond populations through Mulliken analysis and postulated a phase transition path that interpolates between the fivefold and sixfold coordinated structures. Downs *et al.*[11] have studied bond critical point properties in $CaSi_2O_5$ and pointed out a large bond ellipticity in the lengthened Si-O bond (2.8 Å), denoting the impending rupture of this bond. The enthalpy of formation for the transition was measured from calorimetry.[12] Here we focus on the transition mechanism at the atomic scale. We have performed a comprehensive first-principles molecular

dynamics study on $CaSi_2O_5$, including high-pressure structural simulations, lattice dynamics, elasticity, and electron density analysis.

II. METHOD

Our calculation is based on the density functional calculation[13] using the Perdew-Burke-Ernzerhof (PBE) generalized gradient approximation (GGA)[14] form for the exchange correlation functional in combination with the plane-wave pseudopotential method as implemented in the QUANTUM ESPRESSO package.[15] The Troullier and Martins[16] type norm-conserving pseudopotentials were used for Si, O, and Ca. The accuracy of the Si and O pseudopotentials has been demonstrated in previous high-pressure studies on the Mg_2SiO_4 olivine-wadsleyite-ringwoodite system[17] and on the $MgSiO_3$ majorite-perovskite-ilmenite system.[18] The PBE-type Ca pseudopotential was generated using a reference configuration $3s^2 3p^{4.8} 3d^{0.2}$ ($r_c = 2.0$ a.u. for s, p, and d channels, p local), similar to the recipe of Karki and Wentzcovitch.[19] The nonlinear core correction was not used because of the negligible effect on the equation-of-state parameters, a 0.5% increase in volume and a 1% decrease in bulk modulus for CaO. The kinetic energy cutoff for plane waves (E_{cut}) was chosen to be 80 Ry, and a $2 \times 2 \times 2$ [with $(\frac{1}{2}\frac{1}{2}\frac{1}{2})$ shift from the origin] Monkhorst-Pack k-point mesh[20] was used for Brillouin zone samplings of the electronic states. Increasing the k-point mesh to $4 \times 4 \times 4$ and E_{cut} to 90 Ry does not alter equation-of-state parameters or the triclinic to the monoclinic transition pressure. Crystal structures were relaxed under hydrostatic pressures using the variable-cell shape molecular dynamics.[21,22] The dynamical matrices were calculated on a $2 \times 2 \times 2$ q-point mesh, and then interpolated to a denser q-point mesh ($4 \times 4 \times 4$) to obtain the phonon density of states.

III. RESULTS AND DISCUSSION

The triclinic $CaSi_2O_5$ polymorph (space group $I\bar{1}$) was first unambiguously identified by Angel *et al.*[1] through single-crystal x-ray diffraction. The crystals were obtained by synthesis at high pressures and temperatures, and then quenched to ambient conditions to obtain the triclinic phase. This triclinic structure [Fig. 1(a)] is distinctive for the coexisting four-, five- and sixfold coordinated silicon atoms by oxygen. The tetrahedrally-coordinated silicon atoms cross-link the silicate chains formed by corner-sharing SiO_5 and SiO_6 polyhedra. The pentacoordinate Si atoms are separated 2.8 Å away from the dangling oxygen atoms, in contrast with regular Si-O bonds (1.6 Å in tetrahedral and 1.8 Å in octahedral environments). An experimental study[23] showed that, upon compression to 0.2 GPa, each dangling O atom is recaptured by a pentacoordinate Si atom, thus forming an SiO_6 unit. The resulting phase has a monoclinic, titanite ($CaTiSiO_5$)-type structure (space group A2/a) comprising chains of corner-sharing SiO_6 octahedra interconnected through SiO_4 tetrahedra [Fig. 1(b)]. The reverse transition (sixfold to fivefold coordinate) was observed in multi-anvil but not in diamond-anvil experiments, which was attributed to the presence of nonhydrostatic stress in the multi-anvil cell.[23] As the rupture of the Si-O bond in

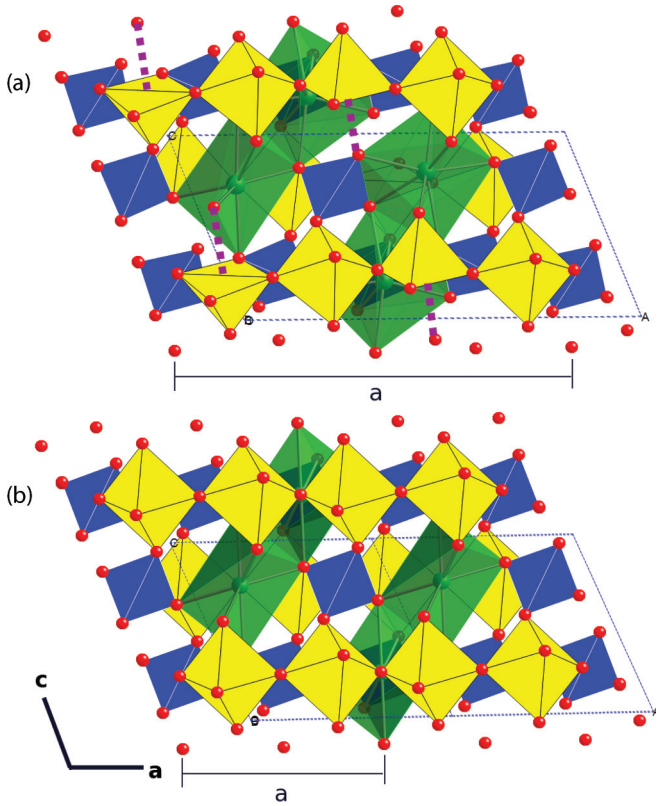

FIG. 1. (Color online) Crystal structures for the two polymorphs of $CaSi_2O_5$: triclinic $I\bar{1}$ (a) and monoclinic A2/a (b). The SiO_5 and SiO_6 units are shown in yellow; SiO_4 tetrahedra are shown in blue; Ca-centered polyhedra are shown in light green; oxygen atoms are shown in red spheres. The dotted lines in (a) denote the hypothetical bonding between Si and O at a distance 2.8 Å. The Ca-O bonds shown here range from 2.2 to 2.5 Å.

$CaSi_2O_5$ is representative of the incipient process for amorphization which is commonly observed in NMR studies,[24] we use *ab initio* molecular dynamics simulations to reveal the microscopic process underlying the transition which is not accessible experimentally.

A. Structural and compressional properties

Our simulations confirm that the triclinic phase is energetically more stable than the monoclinic phase at room pressure. The predicted crystal structure parameters for the two polymorphs at room pressure are compared with results from x-ray diffraction measurements in Table I. The predicted unit cell lengths and cell angles are mostly within one-half percent from experimental values, although GGA overestimates the volume by 1.7% and underestimates the bulk modulus by ~10%, which is well known from previous DFT studies on thermodynamic properties of upper-mantle minerals.[25]

The evolution of the triclinic structure towards monoclinic symmetry is simulated using molecular dynamics. This transition is associated with one quarter of silicon atoms changing their formal or apparent coordination number from 5 to 6. A close view of the local environment surrounding the dangling oxygen atom at room pressure [Fig. 2(a)] shows that it is 2.8 Å away from Si^V (the fivefold coordinated Si) but forms

TABLE I. Crystal cell parameters and equation of states of the two polymorphs of $CaSi_2O_5$, the triclinic phase (space group $I\bar{1}$) and the monoclinic phase (space group A2/a), from the static GGA calculations compared with experiments at room conditions.

Triclinic	a (Å)	b (Å)	c (Å)	α (deg.)	β (deg.)	γ (deg.)	Vol (Å^3)	K (GPa)	K'
GGA	13.03	8.43	6.58	92.59	111.96	90.97	670.07	87.0	4.1
Expt.[a]	12.917	8.450	6.515	93.161	111.48	90.79	660.32		
Monoclinic	a (Å)	b (Å)	c (Å)	β (deg.)	Vol (Å^3)	K (GPa)	K'		
GGA	6.63	8.40	6.41	113.82	326.5	152.0	4.0		
Expt.[b]	6.543	8.392	6.342	113.17	320.10	178.2	4		

[a]Reference 1.
[b]References 23,35.

a regular O-Si bond (1.61 Å) with Si^{IV} (tetracoordinate Si) and at the same time it is connected to two Ca atoms in bond lengths of 2.3 and 2.4 Å, respectively. Upon compression, the elongated Si-O bond shrinks from 2.8 to 1.8 Å but one of the Ca-O distances increases from 2.4 to 3.1 Å [the dashed line in Fig. 2(b)]. This can be interpreted as the breakdown of the Ca-O bond in favor of forming the short Si-O bond (1.8 Å). In addition, the Si-O bond formation is affected not merely from the hopping of the dangling O atom but involves a translation of the whole SiO_4 unit towards the pentahedron [see Fig. 2(b)], indicating the nature of a collaborative transition.

Shown in Fig. 3 are the presssure evolution of the crystal structure parameters and that of the elongated Si-O bond length involved in the transition from GGA calculations. The open symbols connected by the dashed lines represent the simulation starting with a triclinic structure (−4 GPa), whereas the solid straight lines are results starting from a monoclinic structure at high pressures (10 GPa). When compressed from 0 to 2 GPa, the cell parameters of the triclinic phase vary smoothly with pressure, including cell lengths and cell angles; meanwhile the lengthened Si-O distance decreases from 2.8 Å to 2.6 Å [Fig. 3(c)]. A sudden structural variation occurs, however, between 2 and 2.7 GPa, because multiple competing structures were encountered in the simulation that differ in internal shear stress but have very close enthalpy, which apparently have prevented the code from identifying optimal structures that satisfy hydrostatic conditions. This reveals the inability of the triclinic structure to maintain hydrostatic stress with increasing pressures. In addition, no soft phonon modes were found in the triclinic structure even at 2 GPa (see phonon dispersions in the Appendix) in the regime in which the structure is showing bulk softening (see below), indicating that the structure with fivefold coordinated Si is dynamically stable at 2 GPa. This together with the lack of soft phonon modes in the monoclinic structure (the high-pressure phase) from 0 to 5 GPa from this calculation indicates that this transition is not driven by soft phonon modes. What these simulations therefore show, in contrast to the constrained simulations of Warren *et al.*,[10] is that the process is completely reversible and that intermediate structural states, at least up to 2 GPa in these simulations, are stable.

When the pressure exceeds 2.7 GPa, the triclinic phase rapidly converged to the monoclinic titanite structure. The structural parameters at 2.7 GPa are significantly different from those obtained at 2 GPa: the length of the c axis drops from 6.48 to 6.34 Å and that of the a axis increases from 13.0 to 13.15 Å, but the change in the b axis is minute, from 8.40 to 8.37 Å [Fig. 3(a)]. In addition, the β angle increases abruptly from 112.1° to 113.5°, and the other two angles, α and γ, tend to approach 90° [Fig. 3(b)]. The cause of this dramatic structural

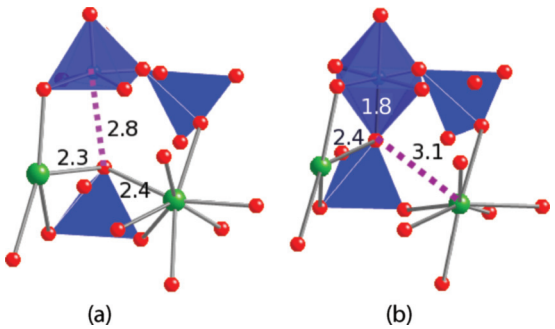

FIG. 2. (Color online) Polyhedral connectivity in $CaSi_2O_5$ at 0 GPa from the simulation: (a) the $I\bar{1}$ phase and (b) the A2/a phase. The bond lengths that are directly involved in the formation of the "sixth" Si-O bond are indicated. The green spheres represent Ca atoms, blue Si, and red O.

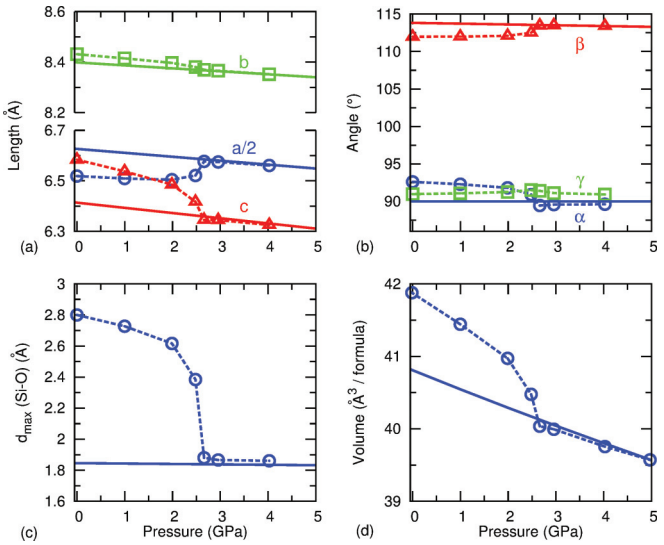

FIG. 3. (Color online) Variation with pressure of cell parameters—(a) cell lengths, (b) cell angles, and (d) cell volumes—across the triclinic (symbols joined by dashed lines) to the monoclinic (solid lines) transition. Also shown is (c) the simulation for the Si-O bond length during its formation process.

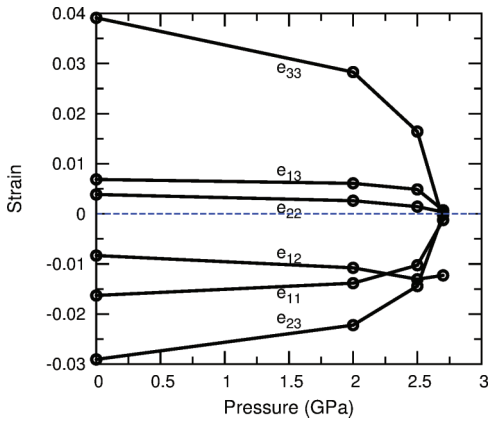

FIG. 4. (Color online) Spontaneous strains for the low-pressure triclinic structure relative to the high-pressure monoclinic structure in $CaSi_2O_5$ (for details see Appendix).

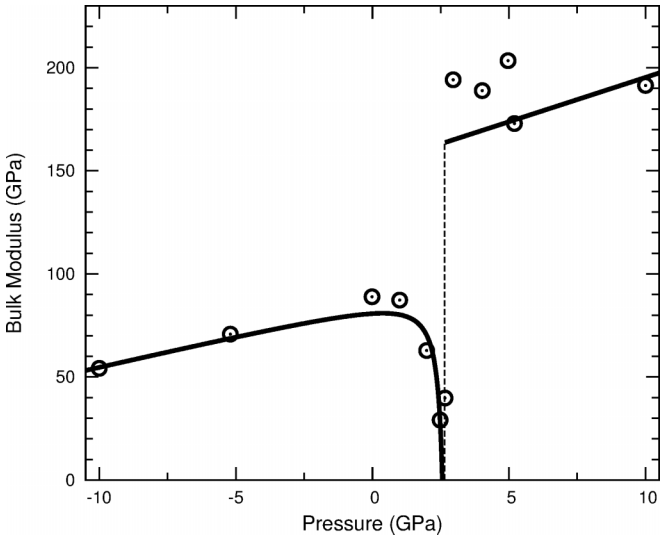

FIG. 5. The calculated bulk modulus of $CaSi_2O_5$ across the triclinic to monoclinic phase transition. The symbols represent the bulk modulus calculated by finite difference between consecutive P, V data points obtained in simulations. Away from the transition, the lines are the EoS fit to the P-V data of the two phases. In the neighborhood of the transition the line is an interpolation between the data points.

change is not just the recovery of the regular Si-O bond (1.8 Å) from the dangling bond state (2.8 Å). The Si-O vector has significant components along both the b and c axes, and so both of these cell parameters decrease. But the formation of the short Si-O bond also increases the intrachain repulsion resulting in an expansion in the chain length (a axis) and further changes in the cell parameters result from the cooperative rotations of all components of the structure.

A deeper understanding of the transition mechanism can be gained by plotting the pressure dependence of the components of the spontaneous-strain tensor (e.g., the GGA results) associated with the symmetry-breaking transition [from monoclinic to triclinic, as defined by Eqs. (38) to (42) in Ref. 26). The results from Fig. 4 show the development of spontaneous strain under decompression. The non-symmetry-breaking strains e_{11}, e_{22}, e_{33}, e_{13}, and e_{23} all evolve linearly with one another, as required by symmetry. At 2.7 GPa, the appearance of the symmetry-breaking strain e_{12} (a nonzero value) corresponds to the discontinuous jump in the γ angle from the simulation [Fig. 3(b)]. At lower pressures, the presence of large axial strains, e_{33} (positive) and e_{11} (negative), correlate with the lengthening of the Si-O bond parallel to the c axis [Fig. 1(a)], which expands the c axis and shrinks the length of the silicate chains (along the a axis). Similarly the large negative shear strain e_{23} develops due to the increase in α angle and c axis. The stronger decrease of e_{22} and especially e_{33} compared to the increase in e_{11} as the transition is approached results in a softening of the structure.

B. Elastic properties

By analyzing the pressure evolution of unit cell volume, we clearly see a structure softening (Fig. 5) accompanying the structure crossover. While at pressures well away from the phase transition the bulk modulus can be described by finite strain equation of state (EoS), there is no adequate method to fit the variation of bulk modulus in the neighborhood of the transition. We have therefore calculated the bulk modulus in this regime by finite difference between P-V calculated by simulations at consecutive pressure points. Such a phenomenon is typical of softening preceding structural phase transitions at high pressures (e.g., Refs. 27 and 28), including softening caused by spin transitions (e.g., Refs. 29). As pressure is increased towards the transition, the bulk modulus of the triclinic phase suddenly drops from 95 GPa to nearly zero, before it bounces back to 163 GPa, the value of the monoclinic phase. This clearly correlates with the contraction of the dangling Si-O bond from 2.8 to 1.8 Å. In fact, this softening is obviously the combined effect of the rapid contraction and softening of the crystallographic b and c directions [Fig. 3(a)], and thus the decrease in e_{22} and e_{33}

TABLE II. Elastic constants of the monoclinic (A2/a) and the triclinic ($I\bar{1}$) $CaSi_2O_5$ at 0 GPa from static GGA calculations, in unit of GPa. The dashes represent strictly zero owing to monoclinic symmetry.

C_{ij}	11	22	33	44	55	66	12	13	14	15	16
A2/a	373.4	414.1	293.3	116.6	75.0	42.3	113.2	53.0	–	0.0	–
Im1	313.7	319.0	158.0	73.8	68.2	67.3	100.0	56.3	3.7	23.4	1.2
C_{ij}	23	24	25	26	34	35	36	45	46	56	
A2/a	26.8	–	0.0	–	–	90.0	–	–	0.0	–	
Im1	59.8	34.6	−3.1	−4.0	47.9	13.0	−11.1	3.0	10.3	1.2	

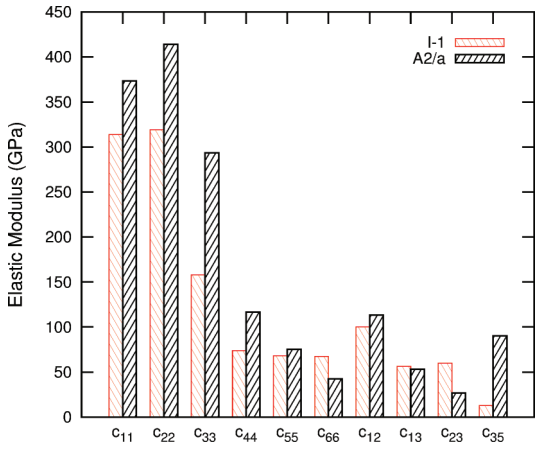

FIG. 6. (Color online) Comparison of the elastic constants for the triclinic phase ($I\bar{1}$) and the monoclinic phase (A2/a) in $CaSi_2O_5$ at 0 GPa from the GGA calculation.

(Fig. 4), as a result of the cooperative rearrangement of the structure described above.

To understand the influence of Si-O bond formation on elasticity, we compare the calculated elastic constants of the two $CaSi_2O_5$ polymorphs (Table II and Fig. 6). Due to structural similarity, some elastic constants, such as c_{11}, c_{55} and c_{12}, are close or of the same order of magnitude for the two polymorphs, as expected, but there are significant differences existing between some other elastic constants. For example, the value of c_{33} of the monoclinic phase is double that of the triclinic phase, c_{35} is six times greater, and c_{44} is 58% greater. This is clearly due to the formation of the extra short Si-O bond ($\sim$1.8 Å) and thus SiO_6 octahedra, which stiffens the crystal structure along the c axis resulting in a large c_{33}, meanwhile increases the response of the axial stress (σ_{33}) to the shear strain in the a-c plane (e_{13}), producing a much larger c_{35}. It is also noted that (Table II) the Cauchy relations which hold for atomic interactions with purely central forces and in a lattice with inversion symmetry[30] are better obeyed in the triclinic phase than in the monoclinic phase. For example, the ratios $c_{23} : c_{44}$, $c_{13} : c_{55}$, and $c_{12} : c_{66}$, which equal 1 according to Cauchy relations, are 0.81 (0.23), 0.83 (0.71), and 1.5 (2.7) in the triclinic (monoclinic) case, respectively.

C. Electron density analysis

Here we discuss features of electron density distributions around the regular octahedral and pentahedral sites, and correlate structure stability with chemical bonding. The polarization of the Si atoms in the triclinic phase is revealed by the Born effective charge tensors. The Z_{33} components of Si in the tetrahedral, pentahedral, and octahedral environments are 3.18, 3.64, and 4.17, respectively (Table III), suggesting that the effective charge transfer amount from Si^V to the dangling oxygen atom is indeed much weaker than from Si^{VI} to its regular oxygen vertex. In the language of quantum chemistry, a bond path can be found along the 2.8 Å Si^V-O connection, but it differs markedly from the regular Si^{VI}-O bonds, as shown in Figs. 7(a) and 7(b) which compare cross sections of the valence electron density through the SiO_5 pentahedron and through the regular SiO_6 octahedron. The valence electron density

TABLE III. Diagonal elements of the Born effective charge tensor of silicon atoms in tetrahedral, pentahedral, and octahedral environments in $CaSi_2O_5$ (see Fig. 1).

Z_{ij}	Si(IV)	Si(V)	Si(VI)
Z_{11}	3.08	3.90	4.11
Z_{22}	3.48	4.05	3.99
Z_{33}	3.18	3.64	4.17

map around Si^{VI} shows a cube-shaped isosurface, which is isotropic towards the six O neighbors [Fig. 7(b)]. The density around the center of the pentahedron, however, displays a bell-shaped isosurface pointing towards the dangling O atom [Fig. 7(a)]. At the bond critical point, a local minimum in density along the elongated Si-O path (2.8 Å) is 0.1 e Å^{-3}, which is much smaller than the minimum density along the regular Si-O bond ($\sim$1.8 Å) in the octahedral environment, 0.3 e Å^{-3}. This is consistent with the previous Hartree-Fock all-electron calculations,[11] which shows that the density values at the bond critical points are 0.85 and 0.1 e Å^{-3} for the regular and elongated Si-O bonds, respectively. Close to the critical point [Fig. 7(a)], the density anisotropy perpendicular to the bond path is clearly seen from the asymmetric contour line at 0.1 e Å^{-3}. A particular measure of this anisotropy is called the bond ellipticity, which is defined as $\epsilon = \lambda_1/\lambda_2$, with λ_1 and λ_2 being the two negative eigenvalues of the Hessian

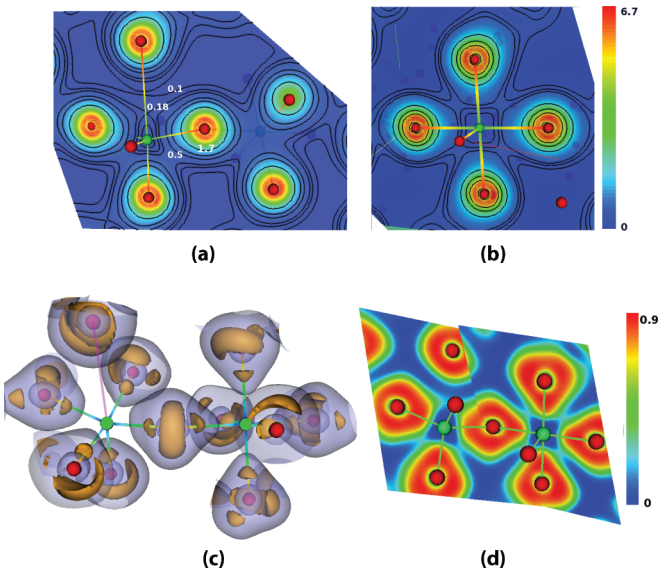

FIG. 7. (Color online) Chemical bonding for the elongated and regular Si-O bonds in the triclinic $CaSi_2O_5$. (a), (b) the valence electron density maps; (c), (d) maps of electron localization function. Si atoms are shown in green spheres and O atoms in red spheres. (a) A cross section through the SiO_5 pentahedron containing the dangling Si-O bond of 2.8 Å; the contour lines for electron density are at 0.1, 0.18, 0.25, 0.5, 0.8, and 1.7 e Å^{-3}. (b) A cross section through a regular SiO_6 octahedron together with the density contour lines at 0.2, 0.3, 0.4, 1.7, 3.35, and 5.0 e Å^{-3}. (c) Isosurfaces of the electron localization function of the corner-sharing SiO_5 (left) and SiO_6 (right), with the inner isovalue at 0.85 and the outer at 0.7. (d) The two cross sections for the electron localization function through Si^V (left) and Si^{VI} (right).

matrix (the second partial derivatives of density with respect to coordinates) at the critical point and in the order of decreasing magnitude. In regular Si-O bonds, $\epsilon \approx 1$, but in the elongated Si-O path it is much larger, 3.55,[11] indicating instability of the bond which is susceptible to rupture.

In addition, the isosurfaces of the electron localization function[31] calculated from the valence electron density are shown in Fig. 7(c). The inner isosurfaces with iso-value 0.85 confines two types of domains: one is shared electron domains represented by small, sphere-shaped density accumulations between bonded Si and O atoms (shown in green lines), and the other is large cone-shaped and torus-shaped domains near O atoms, representing electron lone-pair domains. Clearly, a shared density accumulation domain exists between all Si^{VI}-O bonds but there is no such feature close to the dangling oxygen atom [Fig. 7(c)]. On the contrary, the localization of the SiO_5 unit appears well defined with the dangling oxygen atoms excluded out of their domains as seen from cross sections of the localization function [Fig. 7(d)].

IV. CONCLUSION

We have studied in detail the phase transition mechanism associated with the triclinic to monoclinic transition in $CaSi_2O_5$ from first-principles calculations. Our simulation revealed a transition path from the low pressure phase to the high pressure phase, along which one quarter of silicon atoms change their coordination number from 5 to 6. Accompanying the increase in the coordination number are a decrease in the Si-O distance from 2.8 to 1.8 Å and an increase in the Ca-O distance from 2.4 to 3.1 Å. These bond-length variations are interpreted as a result from the competition for the vertex-oxygen atom between the SiO_5 and the CaO_8 units (Fig. 2). In addition, we emphasize that, not only is the transition accompanied by the displacement of a single oxygen vertex atom, but also by the collective adjustment of adjacent atoms around the SiO_5 pentahedron, such as the SiO_4 group. Although the experimental study shows that the triclinic to monoclinic transition is nearly instantaneous (within a pressure interval less than 0.04 GPa), the molecular dynamics simulation suggests the existence of intermediate structures in which the dangling Si-O distance can be 2.6 Å (at 2 GPa). The phonon calculations at 2 GPa show no signs of soft phonon modes. We also analyzed the spontaneous strain during the monoclinic to the triclinic transition, and find e_{12} being the only dominant symmetry-breaking strain, which corresponds to the discontinuity in the γ angle upon the transition. The elasticity calculation shows that c_{33} and c_{35} of the monoclinic phase are much larger than those of the triclinic phase. This is well rationalized in terms of structure by the formation of the short Si-O bond (1.8 Å) in the monoclinic phase, in contrast the corresponding Si-O distance in the triclinic phase is 2.8 Å. To characterize chemical bonding properties around SiO_5 pentahedra and SiO_6 octahedra, we analyzed the valence-electron density and the electron localization function of the triclinic structure. The elongated Si-O bond is peculiar in that it has a small electron density, but an exceptionally large bond ellipticity at the bond-critical point, which indicates that the bond is weak, and anisotropic in the transverse direction, therefore susceptible to rupture. Clear distinction is observed from maps of the electron localization function between the elongated Si-O bond and the regular Si-O bond; a local maximum exists in the latter bond but not in the former. Nonetheless, despite the interpretation of conventional crystal chemistry that this long Si-O distance does not constitute a "bond" our results show that in this case there is still weak residual interaction between the Si and O, that would presumably be broken on further expansion of the structure.

ACKNOWLEDGMENTS

This work was supported by NSF Grant No. EAR-1118691 and in part by the Alexander von Humboldt foundation. One of us (Y.G.Y.) thanks R. M. Wentzcovitch, S. J. Clark, and C. J. Pickard for helpful discussions. Computations were performed on the Hess cluster at the Geoscience Department at Virginia Tech, for which we are obliged to the courtesy of S. D. King and Y. Zhou. Data analysis was supported in part by ERC starting Grant No. 307322 to F. Nestola.

APPENDIX

1. Spontaneous strain

We have calculated the bulk and shear moduli for the monoclinic $CaSi_2O_5$ using the Reuss theory (see, e.g., Refs. 32 and 33), $K_R = [s_{11} + s_{22} + s_{33} + 2(s_{12} + s_{13} + s_{23})]^{-1}$ and $G_R = 15[4(s_{11} + s_{22} + s_{33}) - 4(s_{12} + s_{13} + s_{23}) + 3(s_{44} + s_{55} + s_{66})]^{-1}$, with the tensor notation denoted in Ref. 34. We have adopted the notion from Carpenter *et al.*[26] to calculate the spontaneous-strain tensor related to the symmetry-breaking transition from the monoclinic to the triclinic phase [Eqs. (38) to (42) in Ref. 26].

2. Phonon dispersions

Phonon dispersions and vibrational density of states of the triclinic structure at 2 GPa from the GGA calculation are shown in Fig. 8.

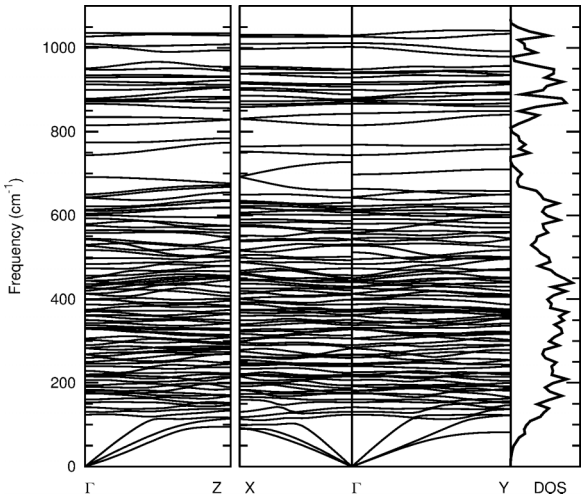

FIG. 8. Phonon dispersions and vibrational density of states of the triclinic $CaSi_2O_5$ at 2 GPa from GGA calculations. X, Y, and Z denote, respectively, the bisecting points of the three reciprocal vectors: b_1, b_2, and b_3.

*yu@kristall.uni-frankfurt.de

[1]R. J. Angel, N. L. Ross, F. Seifert, and T. F. Fliervoet, Nature (London) **384**, 441 (1996).
[2]R. J. Hemley, A. P. Jephcoat, H. K. Mao, L. C. Ming, and M. H. Manghnani, Nature (London) **334**, 52 (1988).
[3]C. Meade and R. Jeanloz, Science **241**, 1072 (1988).
[4]M. B. Kruger and R. Jeanloz, Science **249**, 647 (1990).
[5]Y.-T. Cheng and W. L. Johnson, Science **235**, 997 (1987).
[6]F. Xiong, A. D. Liao, D. Estrada, and E. Pop, Science **332**, 568 (2011).
[7]S. Weiner, I. Sagi, and L. Addadi, Science **309**, 1027 (2005).
[8]T. Irifune, K. Kuroda, N. Funamori, T. Uchida, T. Yagi, T. Inoue, and N. Miyajima, Science **272**, 1468 (1996).
[9]T. A. Mary, J. S. Evans, T. Vogt, and A. W. Sleight, Science **272**, 90 (1996).
[10]M. C. Warren, S. A. T. Redfern, and R. Angel, Phys. Rev. B **59**, 9149 (1999).
[11]R. T. Downs, G. V. Gibbs, M. B. Boisen, Jr, and K. M. Rosso, Phys. Chem. Miner. **29**, 369 (2002).
[12]M. Schoenitz, A. Navrotsky, and N. Ross, Phys. Chem. Miner. **28**, 57 (2001).
[13]W. Kohn and L. J. Sham, Phys. Rev. **140**, A1133 (1965).
[14]J. P. Perdew, K. Burke, and M. Ernzerhof, Phys. Rev. Lett. **77**, 3865 (1996).
[15]P. Giannozzi, S. Baroni, N. Bonini, M. Calandra, R. Car, C. Cavazzoni, D. Ceresoli, G. L. Chiarotti, M. Cococcioni, I. Dabo *et al.*, J. Phys.: Condens. Matter **21**, 5502 (2009).
[16]N. Troullier and J. L. Martins, Phys. Rev. B **43**, 1993 (1991).
[17]Y. G. Yu, V. L. Vinograd, B. Winkler, and R. M. Wentzcovitch, Phys. Earth Planet. Inter. **217**, 36 (2013).
[18]Y. G. Yu, R. M. Wentzcovitch, V. L. Vinograd, and R. J. Angel, J. Geophys. Res. **116**, B02208 (2011).
[19]B. B. Karki and R. M. Wentzcovitch, Phys. Rev. B **68**, 224304 (2003).
[20]H. J. Monkhorst and J. D. Pack, Phys. Rev. B **13**, 5188 (1976).
[21]R. M. Wentzcovitch, Phys. Rev. B **44**, 2358 (1991).
[22]R. M. Wentzcovitch, J. L. Martins, and G. D. Price, Phys. Rev. Lett. **70**, 3947 (1993).
[23]R. J. Angel, Am. Mineral. **82**, 836 (1997).
[24]M. Kanzaki, J. F. Stebbins, and X. Xue, Geophys. Res. Lett. **18**, 463 (1991).
[25]R. M. Wentzcovitch, Y. G. Yu, and Z. Wu, in *Theoretical and Computational Methods in Mineral Physics: Geophysical Applications*, Chap. 4, edited by R. M. Wentzcovitch and L. Stixrude, special issue of Rev. Mineral. Geochem. **71**, 59 (2010).
[26]M. A. Carpenter, E. K. H. Salje, and A. Graeme-Barber, Eur. J. Mineral. **10**, 621 (1998).
[27]J. D. C. McConnell, C. A. McCammon, R. J. Angel, and F. Seifert, Z. Kristallogr. **215**, 669 (2000).
[28]B. Mihailova, R. J. Angel, A.-M. Welsch, J. Zhao, J. Engel, C. Paulmann, M. Gospodinov, H. Ahsbahs, R. Stosch, B. Güttler *et al.*, Phys. Rev. Lett. **101**, 017602 (2008).
[29]Z. Wu, J. F. Justo, C. R. S. da Silva, S. de Gironcoli, and R. M. Wentzcovitch, Phys. Rev. B **80**, 014409 (2009).
[30]M. Born and K. Huang, *Dynamical Theory of Crystal Lattices*, International Series of Monographs on Physics (Clarendon, Oxford, 1956).
[31]A. D. Becke and K. E. Edgecombe, J. Chem. Phys. **92**, 5397 (1990).
[32]R. Hill, Proc. Phys. Soc. London, Sect. A **65**, 349 (1952).
[33]R. J. Angel, J. M. Jackson, H. J. Reichmann, and S. Speziale, Eur. J. Mineral. **21**, 525 (2009).
[34]J. F. Nye, *Physical Properties of Crystals: Their Representation by Tensors and Matrices* (Oxford University Press, Oxford, 1985), Chap. 6.
[35]R. J. Angel, M. Kunz, R. Miletich, A. B. Woodland, M. Koch, and R. L. Knoche, Am. Mineral. **84**, 282 (1999).